



# Effect of process parameters on the deep drawing formability of aluminum and advanced high-strength steel square cups

Iliass El Mrabti<sup>1</sup> · Khalid Bouziane<sup>1</sup> · Abdelhamid Touache<sup>1</sup> · Abdelhadi El Hakimi<sup>1</sup> · Abderrahim Chamat<sup>2</sup> · Abdelmajid Daya<sup>3</sup>

Received: 31 July 2022 / Accepted: 28 November 2022 / Published online: 5 December 2022  
© The Author(s), under exclusive licence to Springer-Verlag London Ltd., part of Springer Nature 2022

## Abstract

Considering the recent high market demand for the use of aluminum and advanced high-strength steel (AHSS) in automotive and aerospace industries, the formability of these materials and comparison with mild steel have been studied. To design a forming tool that produces good quality, it was essential to understand the influence of process variables. In this paper, the significance degree of nine deep drawing parameters, including die section radius, blank holder force, blank thickness, punch section radius, die fillet radius, punch fillet radius, and the three friction coefficients between the tools and blank on the deep drawing characteristics, has been determined. Firstly, a finite element (FE) model is developed for numerical simulation of the deep drawing process using ABAQUS software, and the precision of this model is validated by experimental results. Secondly, due to the high number of parameters, the numerical simulations were performed according to the Taguchi design. Finally, a combination of the analysis of variance (ANOVA) method and Taguchi's signal-to-noise ratio method was used to identify the more significant parameters in the square-drawing process.

**Keywords** Sheet metal forming · Aluminum · Advanced high-strength steel · Formability · Taguchi's signal-to-noise ratio method · ANOVA

## 1 Introduction

Deep drawing is a commonly used sheet metal-forming process, in which a blank is extensively plastically deformed in a die by advancing a punch [1]. Advanced high-strength steels (AHSS) and aluminum are a good choice for deep-drawn parts in order to reduce weight and cost while meeting established safety requirements [2, 3]. However, the usage of these types of materials is restricted by manufacturing limitations such as formability due to the small deformation allowed compared to mild steel. In addition, due to the novelty of these materials, there is a shortage of information about their behavior and formability, which may help

to solve new problems that may occur and shorten the time needed to manufacture the tools. Sheet formability is constrained by the presence of process failures such as fracture, wrinkling, springback, and thinning [4, 5]. These defects are associated with the effect of different factors including the geometric parameters, process parameters, and the mechanical properties of the material [6, 7]. Therefore, understanding the influence and determining the significance degree of these parameters on sheet formability becomes a key challenge in sheet forming development.

For this industry need, Dilmec and Arap [8] used ANOVA to determine the degree of importance of process parameters on the dynamic friction coefficient between the flange and radius regions of the tools and the sheet metal. Kardan et al. [9] used the Taguchi technique and analysis of variance method to investigate the effects of eight process factors on residual stresses in the cylindrical stamping process. The results showed that die shoulder radius, blank thickness, BHF, and punch speed have the greatest influence on the deep drawing characteristics. Jeong et al. [10] evaluated the influence of blank holder gap, die corner radius, and die-punch clearance on excessive thinning and springback

✉ Iliass El Mrabti  
iliass.elmrabti@usmba.ac.ma

<sup>1</sup> Mechanical Engineering Laboratory, Sidi Mohamed Ben Abdellah University, Fez, Morocco

<sup>2</sup> Industrial Techniques Laboratory, Sidi Mohamed Ben Abdellah University, Fez, Morocco

<sup>3</sup> Modeling in Mechanical Energetics and Automatic Systems Laboratory, Moulay Ismail University, Meknes, Morocco

during the deep drawing of an Al-2024-O nose rib. For this purpose, 27 finite element simulations were performed using a full three-level, three-variable factorial design. It was found that the thickness reduction ratio increased with the decrease of blank holder gap and die corner radius; on the other hand, the springback increased with the increase of die-punch clearance and die corner radius. Assuming that the optimization of deep drawing parameters should be performed according to their degree of significance, El Mrabti et al. [11] determined the level of significance of blank holder force, punch speed, and friction coefficients between the tools and the blank on springback. It was found that the friction coefficient between die-blank is the most important parameter, while the coefficient of friction punch-blank has less influence in this case.

In the open literature, most attention has been focused on the deep drawing of circular geometry, whilst studies on the deep drawing of square cups are rather lacking. Ayari et al. [12] proposed a parametric study that can be used mainly to control the forming failures. In this paper, the influence of selected parameters such as die and punch radius, shoulder radius, part aspect ratio, and blank holder force on thinning phenomena and thickness distribution along the critical paths has been studied. Singh et al. [13] studied the influence of process parameters in the square cup by the Taguchi and ANOVA methods. It is concluded that coefficient is the most influential and dominant parameter, followed by punch speed and holding force. Regarding the advanced high-strength steel (AHSS) into the rectangular deep drawing process, Regueras and López [14] studied the effect of blank thickness and punch length to width ratio on fracture and thinning for mild steel and AHSS in rectangular stamping using a finite element model. It concluded that an overall increase in thickness creates an increase in the percentage of thickness reduction in the final part and that a small influence of LD can be seen in the drawing process. Choudhari and Khasbage [15] used numerical and experimental approaches to analyze the effect of blank thickness, loading, and lubrication on thinning and wrinkling for the square cup stamping process. The results show that for the process parameters considered, the formability of the material with a blank thickness of 2 mm is better than that of a blank thickness of 1 mm and 0.8 mm, for a load of 100 kN with dry lubrication.

After reviewing the literature, no studies have been published to investigate the influences of multiple parameters on the minimization of rupture and thinning in the deep drawing process of the square cup. In this research article, a survey examining the simultaneous effect of nine different parameters on fracture and thinning in stamped parts and obtaining their degree of significance is presented for the first time. Blank thickness, die section radius, blank holder force, die section radius, punch section radius, punch fillet radius, die fillet radius, and the three friction

coefficients between the tools and blank are the nine main input parameters considered in this research. For this purpose, aluminum and advanced high strength steel (AHSS), which are the most widely used structural materials in the automotive and aerospace industries, were considered. At the same time, a typical mild steel, widely used in the deep drawing process, was also analyzed to compare its formability with that of the other two materials. The ANOVA is used to estimate the percentage of importance of these parameters on the formability of the sheet.

## 2 Methodology

To evaluate the influence of the factors and estimate their percentage of importance on the formability of the sheet, the Taguchi signal-to-noise ratio method and the analysis of variance (ANOVA) were used. The data necessary for this investigation are defined and planned according to the design of experiments (DoE). The main advantage of these designs is the orthogonal arrays technique in which the effects of multiple factors on output characteristics can be estimated simultaneously. According to the literature, there are several kinds of DoE such as full factorial, central composite design (CCD), Box-Behnken design (BBD), and Taguchi [16]. In this study, The experiments are planned according to the Taguchi design [17]. This is motivated by the reason that this experimental design uses special orthogonal arrays that allow a large reduction in the overall number of experiments ordered and thus saving time and resources. Equation 1 shows the way to calculate the minimum number of experiments to perform. The selection of the factors is based on a few preliminary experiments and a review of the literature on the subject. The selection of the levels and intervals of these parameters is based on the industrial values.

$$N_m = F + \sum_{j=1}^F (L_j - 1) \quad (1)$$

where  $N_m$  is number of experiments,  $L_j$  number of levels of parameter  $j$ , and  $F$  number of factors. To investigate the results, the Taguchi technique employs a statistical indicator of performance known as the signal-to-noise ratio (S/N). This indicator takes into consideration the mean and the variability at the same time, and its formula depends on the criteria of the quality feature to be studied. There are four types of S/N ratios for the study of characteristics, namely, the small ratio is the best (LB), the nominal ratio is the best (NB), and the highest ratio is the best (HB). The mathematical formulas of the S/N ratios can be expressed as:

$$\left\{ \begin{array}{l} \text{case of larger is the best, } \frac{S}{N} \text{ ratio} = -10 * \log_{10} \left( \frac{1}{n} \sum \frac{1}{Y^2} \right) \\ \text{case of smaller is the best, } \frac{S}{N} \text{ ratio} = -10 * \log_{10} \left( \frac{1}{n} \sum Y^2 \right) \\ \text{case of nominal is the best, } \frac{S}{N} \text{ ratio} = -10 * \log_{10} (s^2) \end{array} \right. \quad (2)$$

where  $Y$  is the responses for the given factor level combination,  $n$  the number of responses in the factor level combination, and  $s$  the standard deviation of the responses for all the noise factors for the given factor level combination. Since we want to minimize and eliminate the defects encountered during the stamping process, the small ratio is the best (LB) is selected in this study. After carrying out the statistical examination of the  $S/N$  ratio, the analysis of variance (ANOVA) can be contributed at this stage to calculate the variance of the errors and to estimate the relative importance of the factors. It is a statistical method to estimate the percentage of importance for each input variable on the output characteristic. First, the total sum of the squared deviations SST from the total mean  $S/N$  ratio can be calculated by Eq. 4. The sum of the squares due to the variation from the total mean  $S/N$  ratio for the  $P_{th}$  parameter is expressed by Eq. 5:

$$SS_T = \sum_{i=1}^m \left( \frac{S}{N} \right)_i^2 - \left[ \sum_{i=1}^m \left( \frac{S}{N} \right)_i \right]^2 \quad (3)$$

$$SS_p = \sum_{j=1}^l \frac{\left( \frac{S}{N} \right)_j^2}{t} - \frac{1}{m} \left[ \sum_{i=1}^m \left( \frac{S}{N} \right)_i \right]^2 \quad (4)$$

$$P_c(\%) = \frac{SS_p}{SS_T} * 100 \quad (5)$$

where  $m$  is the number of experiments in the orthogonal array and  $(S/N)_i$  is the  $S/N$  ratio of the  $i_{th}$  experiment, where  $l$  is the number of parameter levels ( $l=3$  in this study),  $j$  is the level number of that specific parameter  $p$ ,  $\left( \frac{S}{N} \right)_j^2$  is the sum of the  $S/N$  ratio involving this parameter and level  $j$ , and  $t$  is the repetition of each level of parameter  $p$ .

### 3 DoE and description of case study

The square cup deep drawing problem suggested by the Numisheet'93 conference, as illustrated in Fig. 1, was chosen as case study in this paper. All details of the experiments are reported by Joachim Danckert [18]. The crucial point of this selection is that this kind of deep-drawn part is subject to numerous defects namely wrinkling rupture and thinning [19]. In the square cup forming process, a sheet metal blank with a thickness of 0.78 mm is initially pressed between the die and the blank holder by imposing a holder force of 19.6 kN, and the coefficient of friction is set at 0.144 during the drawing operation. This friction coefficient value is estimated to simulate the real contact between the tools and the sheet metal; similar with each experience, both sides of the white sheet metal surface were dried with a paper towel dipped in the lubricant, and they were kept in a vertical position for 30 min [18]. Analysis of the square cup stamping was performed to obtain a punch stroke of 15 and 40 mm. There are many parameters, including process and material factors, associated with critical process failures

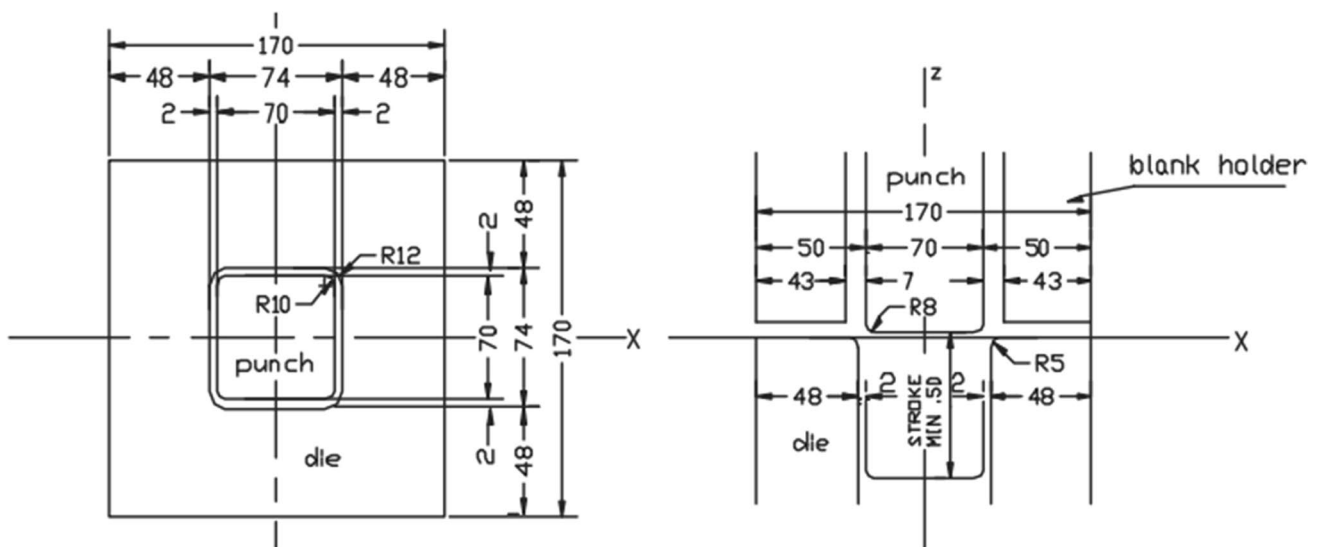


Fig. 1 Profile of square deep drawing problem

such as rupture, wrinkling, and thinning in the deep drawing process. For this reason, nine parameters are considered in this study namely friction coefficient between blank-die ( $\mu_d$ ), punch section radius ( $R_{sp}$ ), blank holder force ( $BHF$ ), die section radius ( $R_{sD}$ ), die fillet radius ( $R_{fD}$ ), punch fillet radius ( $R_{fp}$ ), blank thickness ( $t_b$ ), and the friction coefficient between punch-blank ( $\mu_p$ ) and blank holder-blank ( $\mu_h$ ). The ranges and levels of these parameters are chosen according to the range of values used in the industry and are given in Table 1. As indicated in Table 8 in the Appendix, Taguchi’s design concept proposes an L27 orthogonal table for nine factors each with three levels.

### 4 Finite element model

Faced with today’s competitive challenges, numerical simulation using the finite element method has become an indispensable choice for researchers and manufacturers in various sectors [20–22]. Currently, FE is the principal technique to simulate and analyze the deep drawing process for investigating the interaction between the input factors and the output response. The non-linearity of the behavior laws, the presence of elastoplastic transitions, and the varying boundary conditions of the frictional contact make a precise numerical prediction complicated. A 3D finite element model is developed in the ABAQUS software to simulate the forming operation. Due

to the symmetry of case study, only the fourth has been considered to reduce the calculation time needed. Deep drawing simulations are performed by the dynamic explicit calculation. The S4R shell element with eleven integration points is chosen to discretize the blank, and the discrete rigid element R3D4 is utilized to discretize the die, the punch, and the blank holder. The three contact pairs were defined by the surface-to-surface technique in which Coulomb’s friction law was assumed. The mechanical behavior of the three materials was defined as elastoplastic. To account for the anisotropy of the sheet metal, Hill’s model was used, and for the material hardening models were defined by the Swift isotropic hardening model. Figure 2 illustrates the stress–strain curves of the materials used. The mechanical data for different materials used are shown in Table 1. Figure 3 illustrates a view of the FEM of a square cup and the final piece shape.

To validate the finite element model, two evaluations that examine the final shape of the stamped part are performed. In this study, the final shape of this part, as represented by the stretched length  $DX$ ,  $DY$ ,  $DD$  of the flange, is determined according to Fig. 4. The first one consists in establishing a convergence study of the mesh. Table 2 lists the results of the mesh refinement study with the different mesh densities used. As shown in Table 3, the dimensions of the drawn length ( $DX$ ,  $DY$ ,  $DD$ ) are sensitive to mesh size variation, but above a mesh size of  $60 \times 60$  elements, these dimensions remain unchangeable. For this reason, we set this mesh size for the rest of this work. The second one consists in comparing the simulation and experimental results. The numerical results and experimental data are presented in Table 4. It can be clearly seen that the numerical model is able to predict the experimental data accurately.

Two defects are selected to evaluate the quality of the stamped part in this research. Fracture and thinning are chosen because they are considered the main defects present in square stamped parts and restrict the use of AHSS and aluminum. The forming limit diagram (FLD) is used to characterize the rupture and thinning defined as the thickness variation of the blank after the deep drawing operation. As illustrated in Fig. 5, FLD, which was originally proposed by Keeler [23], shows the limit strains at the initiation of necking. The major and minor strains mapped out in a FLC are derived from formability tests under different strain paths, from uniaxial to biaxial to planar tensile. The region below FLC  $\emptyset(\epsilon_2)$  represents the safe forming area, while the region above the FLC

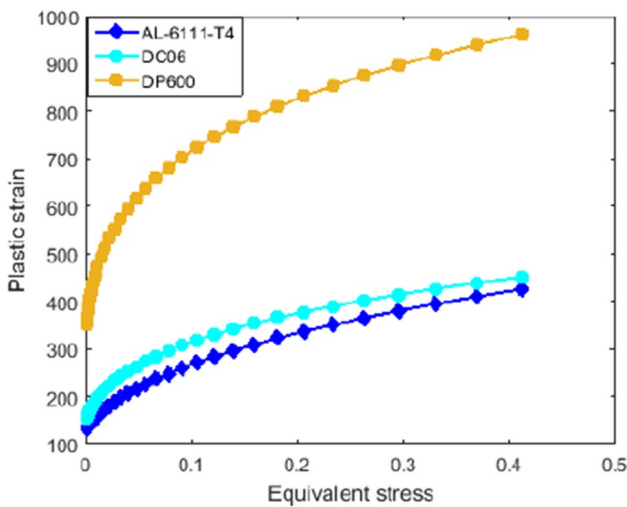


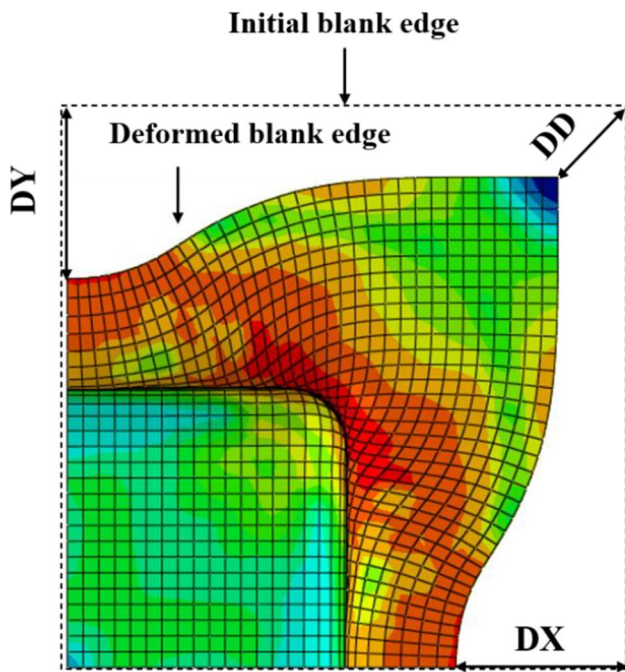
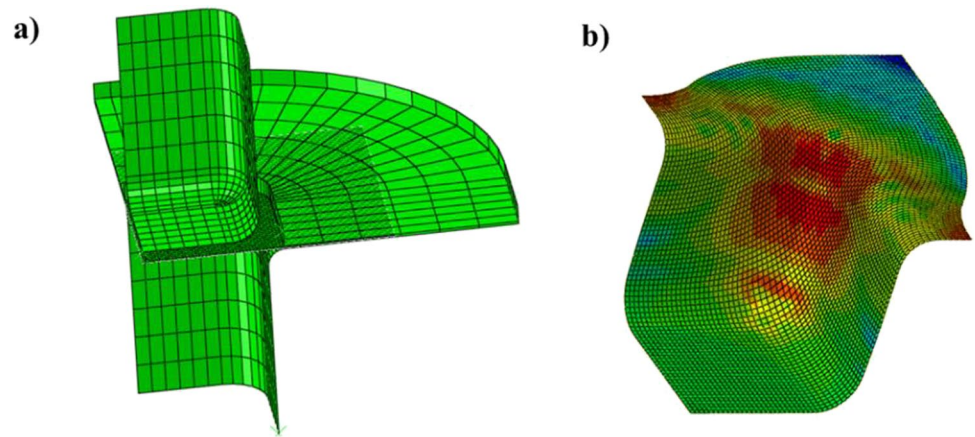
Fig. 2 Stress/strain curves

Table 1 The utilized design variables levels

Variable	$BHF(KN)$	$\mu_p$	$\mu_d$	$\mu_h$	$R_{sp}(mm)$	$R_{sD}(mm)$	$R_{fD}(mm)$	$R_{fp}(mm)$	$t_b(mm)$
Lower	10	0.1	0.05	0.05	8	10	4	6	0.8
Middle	30	0.2	0.15	0.15	12	14	6	10	1.2
Upper	60	0.3	0.25	0.25	16	18	8	14	1.6



**Fig. 3** **a** View of FEM of deep drawing problem; **b** final shape of the sheet



**Fig. 4** Definition of draw-in direction

**Table 2** Mechanical characteristics of different materials concerned

Property	Symbol	Material		
		DP600	AL-6111-T4	DC06
Young modulus (Gpa)	$E$	210	71	206
Poisson ratio	$\nu$	0.3	0.33	0.3
Strain hardening exponent	$n$	0.212	0.3593	0.2637
Strength coefficient (Mpa)	$k$	1157.6	576.79	567.29
Initial strain	$\epsilon_0$	0.00361	0.01658	0.007127
Lankford's coefficients	$r_{0^\circ}$	1	0.71	1.79
	$r_{45^\circ}$	0.8	0.58	1.51
	$r_{90^\circ}$	1.3	0.7	2.27

**Table 3** Mesh convergence study

	30×30 of elements	40×40 of elements	60×60 of elements	75×75 of elements	90×90 of elements
$DX$ (mm)	27.73	25.29	27.14	27.14	27.14
$DY$ (mm)	26.43	26.60	28.42	28.42	28.42
$DD$ (mm)	17.25	17.47	16.69	16.69	16.69

means that a fracture can potentially occur [24]. The FLD curves for the studied materials are displayed in Fig. 6. The ABAQUS software provides the damage initiation criterion FLDCRT which based on these formae limit curves calculated by the Eq. 7. This criterion is defined as the ratio of the current major principal strain (calculated numerically by Abaqus) to the major limiting strain of the FLC as defined in Eq. 10. A value of 1 or greater indicates that damage is occurring and how much the initiation criterion has been exceeded. Then, the two defects are calculated according to the following Eqs. (7, 8).

$$FLDCRT = \frac{\epsilon_{Major}}{\epsilon_{Major}^{FLD}} \tag{6}$$

$$Rupture = \sum_{i=1}^n FLDCRT \tag{7}$$

$$Thinning = \sqrt{\sum_{i=1}^n \frac{(t_0 - t_i)^2}{t_0}} \tag{8}$$

where  $n$  is the number of elements to be tested;  $t_0$  is the initial thickness of the sheet;  $t_i$  is the final thickness of the sheet.

**Table 4** Comparison between simulation results and experimental results

Punch travel (mm)	DX (mm)		DY (mm)		DD (mm)	
	FEM	Exp	FEM	Exp	FEM	Exp
15	6.11	5.64	5.50	6.63	4.02	3.09
40	27.14	27.95	28.42	29.24	16.69	15.84

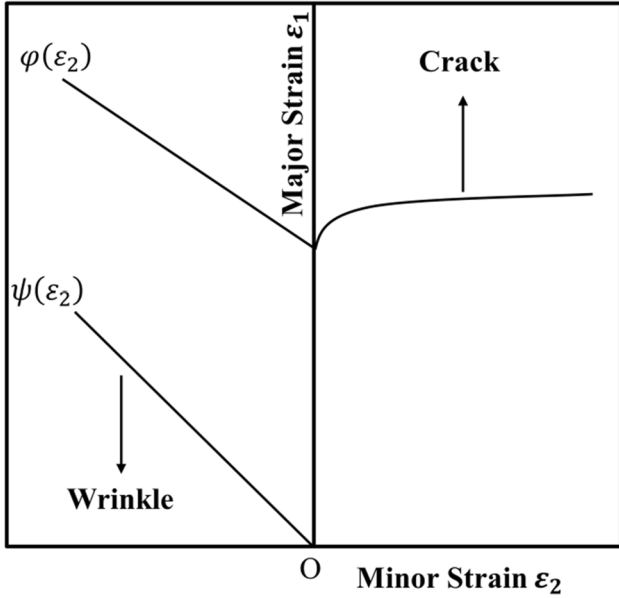


**Fig. 5** Forming limit diagram

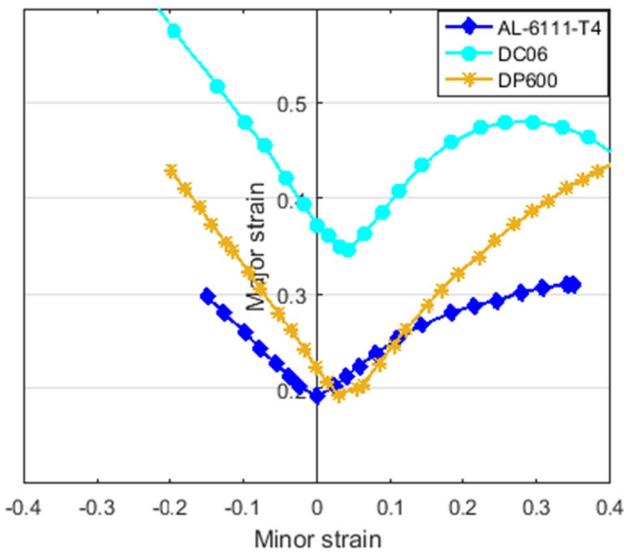


**Fig. 6** FLD for the studied materials [14]

**Table 5** Formability comparison between different materials

Exp. no	MaxFLCDRT results		
	DP600	AL-6111-T4	DC06
1	0.91	1.08	0.59
2	0.87	0.66	0.59
3	0.83	0.53	0.55
4	0.93	1.06	0.65
5	0.92	0.81	0.62
6	0.89	0.72	0.60
7	1.11	1.14	0.74
8	1.11	1.55	0.76
9	0.94	0.78	0.63
10	1.19	0.90	0.67
11	0.94	0.89	0.66
12	0.97	0.63	0.74
13	1.05	0.89	0.67
14	1.11	1.02	0.81
15	1.13	1.61	0.74
16	0.86	0.73	0.59
17	0.96	1.20	0.61
18	0.89	0.85	0.61
19	11.88	4.46	6.07
20	0.91	0.70	0.79
21	1.21	1.73	2.55
22	1.08	1.46	0.82
23	0.80	0.54	0.54
24	1.06	1.27	0.66
25	5.93	0.95	5.50
26	1.07	1.05	0.59
27	0.96	1.41	0.70

## 5 Results and discussion

### 5.1 Formability comparison between different materials

To compare the formability of materials, we used the maximum value of *FLDCRT* as mentioned in Eq. (9):

$$MaxFLCDRT = \max_{0 \leq i \leq n} (FLDCRT) \tag{9}$$

Table 5 presents *maxFLCRT* values of 27 experiments for the studied materials. The results indicate that for the case of DP600 steel and aluminum, 13 and 11 experiments have damage, respectively. While for the case of DC06 steel, only 3 experiments have damage. In other words, the percentage of experiments that show damage is 48.15, 40.74, and 11.12% for the case of AL-6111-T4, DP600, and DC06, respectively. The results give a very clear picture of the great difference between the formability of DP600 and AL on the one hand and mild steel on the other.

### 5.2 Effect of design variables on rupture

Table 9 in the Appendix shows the simulation results for the rupture and the corresponding *S/N* ratios. The effects of nine design variables on the mean value of rupture for the different materials are shown in Figs. 7, 8, and 9. For DP600 and AL-6111-T4 cases, it is clear that the rupture tends to increase with an increase in the friction coefficient between blank and die ( $\mu_d$ ) and blank holder force (*BHF*). These results can be explained by the fact that the increase in holding force results in more pressure on the surface of the material, which prevents the material from flowing and

subjects it to more stress, resulting in rupture [19]. Similarly, a direct relation exists between the mean value of the rupture and friction coefficient between blank and blank-holder ( $\mu_h$ ). On the other hand, it increased with the decrease of friction coefficient between blank and punch ( $\mu_p$ ), die fillet radius ( $R_{fD}$ ), and punch fillet radius ( $R_{fP}$ ). The probable reason for the effect of the fillet radii of the die and punch on the fracture values can be explained by the bending moment of the material. The higher these radii, the easier the material bends. It can be seen that the friction coefficients have different effects on the variation of the mean rupture value, due to the fact that the friction conditions between die/blank and between blank holder/blank are kinematic, while the type of friction between the punch and the blank is static [9]. While, there is no significant variation of the mean rupture values between the different levels of the radius die section radius ( $R_{sD}$ ) and the punch section radius ( $R_{sP}$ ).

For DC06 case, the effect of blank holder force (*BHF*), friction coefficient between blank/die ( $\mu_d$ ), friction coefficient between blank/blank-holder ( $\mu_h$ ), coefficient between blank/punch ( $\mu_p$ ), die fillet radius ( $R_{fD}$ ), and punch fillet radius ( $R_{fP}$ ) is same for DP600 and AL-6111-T4 cases. However, in this case, the effect of blank thickness ( $t_b$ ),

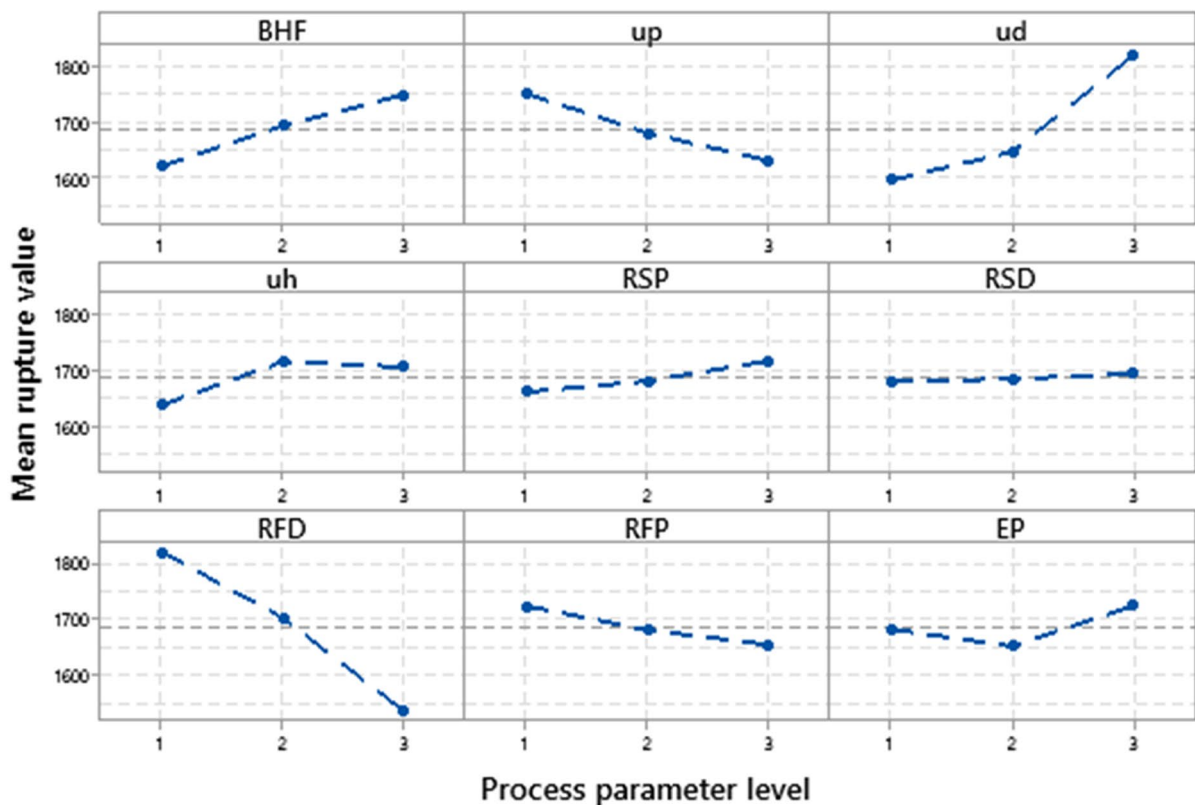
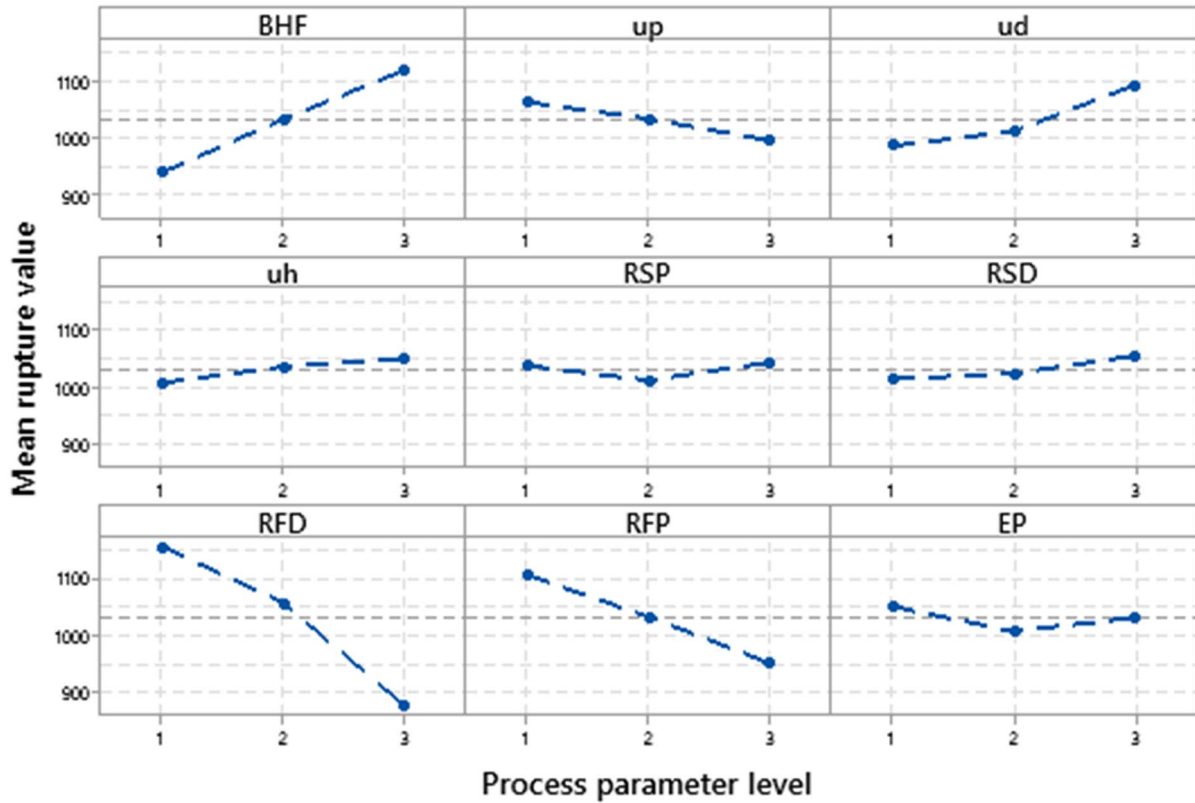


Fig. 7 Main effect of design variables on rupture for DP600 case



**Fig. 8** Main effect of design variables on rupture for AL-6111-T4 case

die section radius ( $R_{sD}$ ), and punch section radius ( $R_{sP}$ ) is very clear. From Fig. 10, it is clear that the rupture tends to increase with the increase of the punch section radius, while it tends to decrease with the increase of the blank thickness and die section radius.

ANOVA is used to identify the more significant parameters that have an effect on rupture and thinning. The results for the analysis of variance regarding rupture for the different materials are presented in Table 6. In addition, this table gives the degree of effect of each input parameter on the rupture as a percentage.

For DP600 steel case, it is clear that the die fillet radius ( $R_{fD}$ ) has the most effect on rupture with 45.13%, followed by the friction coefficient between blank and die ( $\mu_d$ ) with 28.54%. After  $\mu_d$ , the blank holder force ( $BHF$ ) and friction coefficient between blank and punch ( $\mu_p$ ) are the third and fourth parameters which have the most influence on the rupture with 7.78 and 7.21%, respectively. Friction coefficient between blank and blank-holder ( $\mu_h$ ), Punch section radius ( $R_{sP}$ ), and blank thickness ( $t_b$ ) have little effect on rupture, and die section radius ( $R_{sD}$ ) has no effect.

For AL-6111-T4 case, the die fillet radius ( $R_{fD}$ ) was found to be the major factor affecting rupture (52.13%), while punch section radius ( $R_{sP}$ ), die section radius ( $R_{sD}$ ), and friction coefficient between blank and blank-holder ( $\mu_h$ ) had almost no effect on rupture. After  $R_{fD}$ , blank thickness ( $t_b$ ), blank holder force ( $BHF$ ), and punch fillet radius ( $R_{fP}$ ) are the second, third, and fourth most influential parameters on rupture with 18.51, 18.51, and 15.41%, respectively. Friction coefficient between blank and blank-holder ( $\mu_h$ ) and friction coefficient between blank and punch ( $\mu_p$ ) have little effect on rupture.

For DC06 case, it can be seen that the die fillet radius ( $R_{fD}$ ) is again the most significant stamping parameter to affect the rupture (20.76%), followed by the friction coefficient between blank and die ( $\mu_d$ ) with 18.63%. Friction coefficient between blank and blank holder (10.48%), friction coefficient between blank and punch (11.56%), punch section radius (13.26%), and blank thickness (8.84%). Punch fillet radius ( $R_{fP}$ ), die section radius ( $R_{sD}$ ), and blank holder force ( $BHF$ ) are the least significant parameters influencing rupture.



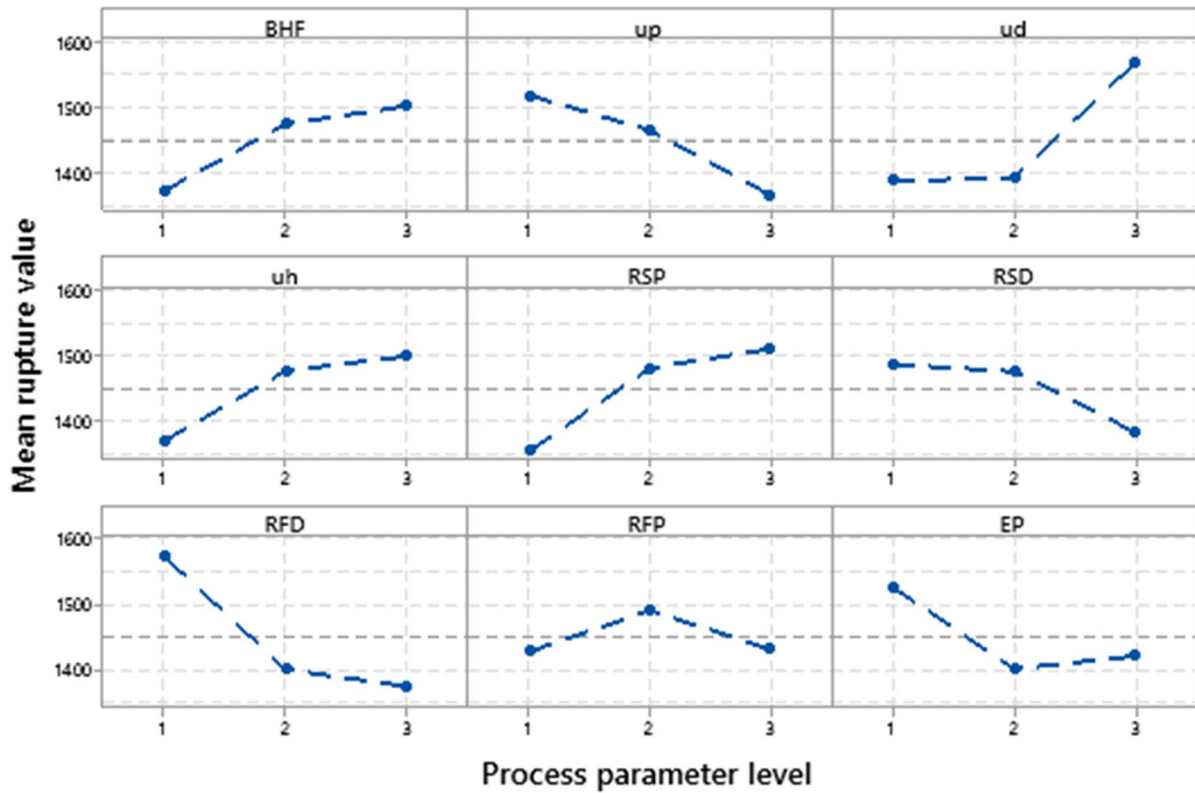


Fig. 9 Main effect of design variables on rupture for DC06 case

### 5.3 Effect of design variables on thinning

Table 10 in the Appendix shows the simulation results for the thinning and the corresponding *S/N* ratios. The effects of nine design variables on the mean value of thinning for the different materials are shown in Figs. 10, 11, and 12. For DP600 steel case, it is clear that the thinning tends to increase with an increase in the friction coefficient between blank and die ( $\mu_d$ ) and blank thickness ( $t_b$ ). The effect of blank thickness on thinning was compared with the results of López and Regueras [25] for square section deep drawing of sheets. The comparison indicated that with an initial increase in thickness creates an increase in the percentage of thickness variation in the final part. Similarly, a direct relation exists between the mean value of the thinning and the blank holder force (*BHF*) and die section radius ( $R_{sd}$ ). Although there is a deviation in the curve, the inverse relation exists between the mean value of thinning and die fillet radius ( $R_{fd}$ ). In other words, the mean value of thinning increases slightly when  $R_{fp}$  increases from 4 to 6 mm, while this amount decreases sharply when going from 6 to 8 mm. Figure 11 also shows great decreases when the punch section radius ( $R_{sp}$ )

increases from 8 to 12 mm. However, this amount will be increased more slightly by increasing the punch section radius from 12 to 16 mm. On the other hand, there is no significant variation of the mean thinning values between the different levels of the punch fillet radius ( $R_{fp}$ ), friction coefficient between blank and punch ( $\mu_p$ ), and friction coefficient between blank and blank-holder ( $\mu_h$ ).

According to Figs. 11 and 12, the deep drawing parameters have the same influence on the thinning for aluminum and high strength steel. However, in AL-6111-T4 case, the effect of radius punch fillet radius ( $R_{fp}$ ), friction coefficient between blank and punch ( $\mu_p$ ), and friction coefficient between blank and blank-holder ( $\mu_h$ ) is very clear. From Fig. 12, it is clear that the thinning tends to increase with the increase of  $\mu_h$ , while it tends to decrease with the increase of the blank thickness  $R_{fp}$  and  $\mu_p$ . According to Figs. 10, 11, and 12, the higher the material strength, the lower the thinning value [14].

The results for the analysis of variance regarding thinning for the different materials are presented in Table 7. For DP600 steel case, it is clear that the blank thickness ( $t_b$ ) has the most effect on thinning with 60.16%, followed by the die fillet radius ( $R_{fd}$ ) with 15.05%. After  $R_{fd}$ , the

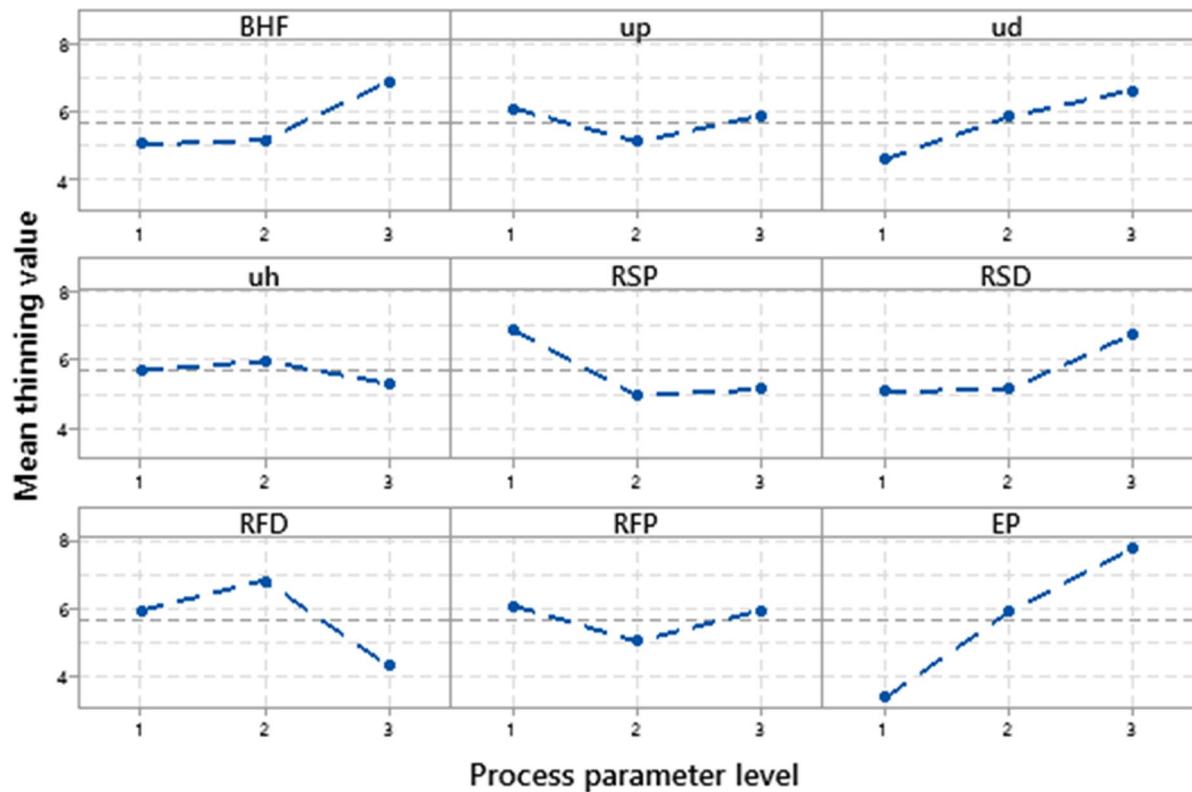


Fig. 10 Main effect of design variables on thinning for DP600 case

Table 6 Analysis of variance for rupture results

Factors	DP600			AL-6111-T4			DC06		
	Sum of squares	P value	%	Sum of squares	P value	%	Sum of squares	P value	%
$BHF$	1.719	0.02	7.778	9.827	0.000	18.514	2.267	0.262	6.161
$\mu_p$	1.593	0.02	7.210	1.299	0.022	2.447	4.255	0.108	11.564
$\mu_d$	6.308	0.00	28.545	4.367	0.001	8.227	6.854	0.043	18.627
$\mu_h$	0.792	0.09	3.582	0.637	0.100	1.200	3.855	0.127	10.477
$R_{sP}$	0.404	0.24	1.827	0.205	0.410	0.386	4.879	0.084	13.260
$R_{sD}$	0.006	0.98	0.026	0.312	0.276	0.588	2.653	0.217	7.210
$R_{fD}$	9.973	0.00	45.129	27.639	0.000	52.072	7.639	0.033	20.760
$R_{fP}$	0.684	0.11	3.096	8.178	0.000	15.408	1.141	0.482	3.101
$t_b$	0.620	0.13	2.805	0.615	0.107	18.514	3.253	0.165	8.841

friction coefficient between blank and die ( $\mu_d$ ) is the third parameter which has the most influence on the thinning with 9.03%. Blank holder force ( $BHF$ ), die section radius ( $R_{sD}$ ), and punch section radius ( $R_{sP}$ ) have little effect on thinning. The radius punch fillet radius ( $R_{fP}$ ), friction coefficient between blank and punch ( $\mu_p$ ), and friction coefficient between blank and blank-holder ( $\mu_h$ ) have almost no effect in this case.

For AL-6111-T4 case, the blank thickness ( $t_b$ ) has the most effect on rupture with 31.28% followed by the die fillet radius ( $R_{fD}$ ) with 21.95%. After  $R_{fD}$ , the friction coefficient between blank and die ( $\mu_d$ ), friction coefficient between blank and punch ( $\mu_p$ ), and blank holder force ( $BHF$ ) is the third parameter which has the most influence on the thinning with 9.03%. The radius of the punch fillet ( $R_{fP}$ ), die section radius ( $R_{sD}$ ), punch section radius ( $R_{sP}$ ), and friction

**Table 7** Analysis of variance for thinning results

Factors	DP600			AL-6111-T4			DC06		
	Sum of squares	P value	%	Sum of squares	P value	%	Sum of squares	P value	%
<i>BHF</i>	17.805	0.022	4.899	43.413	0.000	12.257	22.404	0.001	7.434
$\mu_p$	3.724	0.314	1.025	46.971	0.000	13.262	13.833	0.006	4.590
$\mu_d$	32.940	0.004	9.063	59.824	0.000	16.891	43.091	0.000	14.299
$\mu_h$	1.425	0.616	0.392	4.667	0.024	1.318	3.857	0.114	1.280
$R_{sp}$	14.511	0.035	3.993	0.958	0.331	0.270	2.370	0.231	0.786
$R_{sd}$	14.857	0.033	4.088	0.460	0.566	0.130	4.636	0.082	1.538
$R_{fd}$	54.695	0.001	15.049	77.737	0.000	21.948	39.740	0.000	13.187
$R_{fp}$	4.834	0.235	1.330	9.350	0.004	2.640	2.570	0.208	0.853
$t_b$	218.663	0.000	60.162	110.808	0.000	31.285	168.861	0.000	56.033

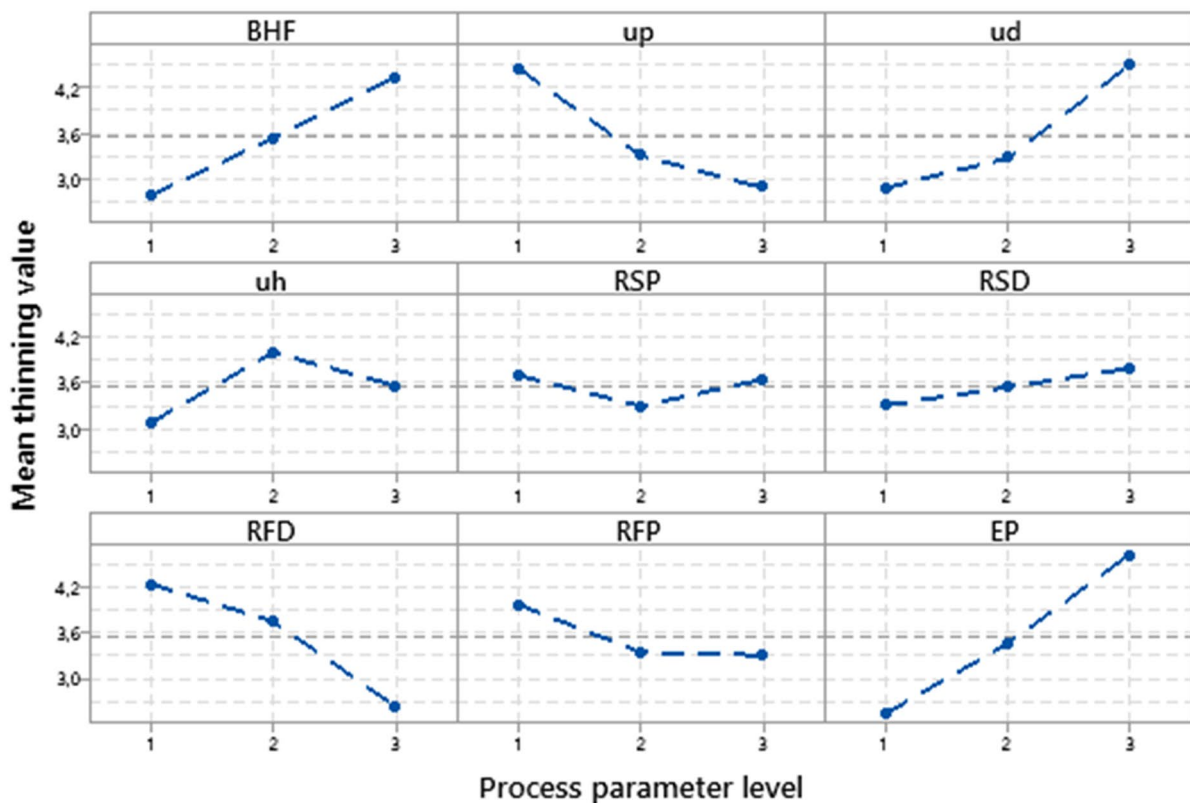


**Fig. 11** Main effect of design variables on thinning for AL-6111-T4 case

coefficient between blank and blank-holder ( $\mu_h$ ) have little or no effect on thinning.

For DC06 case, the blank thickness ( $t_b$ ) has the most effect on thinning with 56.03% followed by the friction coefficient between blank and die ( $\mu_d$ ) and the die fillet radius ( $R_{fd}$ ) with 14.26 and 13.19%, respectively. Friction coefficient between blank and punch ( $\mu_p$ ) and blank holder force (*BHF*) have little effect on thinning. The radius of the punch fillet ( $R_{fp}$ ), die section radius ( $R_{sd}$ ), punch section radius ( $R_{sp}$ ), and friction

coefficient between blank and blank-holder ( $\mu_h$ ) have no effect on thinning (Table 7).

## 6 Conclusions

This paper presents the use of FEM with a combination of analysis of variance (ANOVA) and Taguchi’s signal-to-noise method to identify the more significant parameters in square

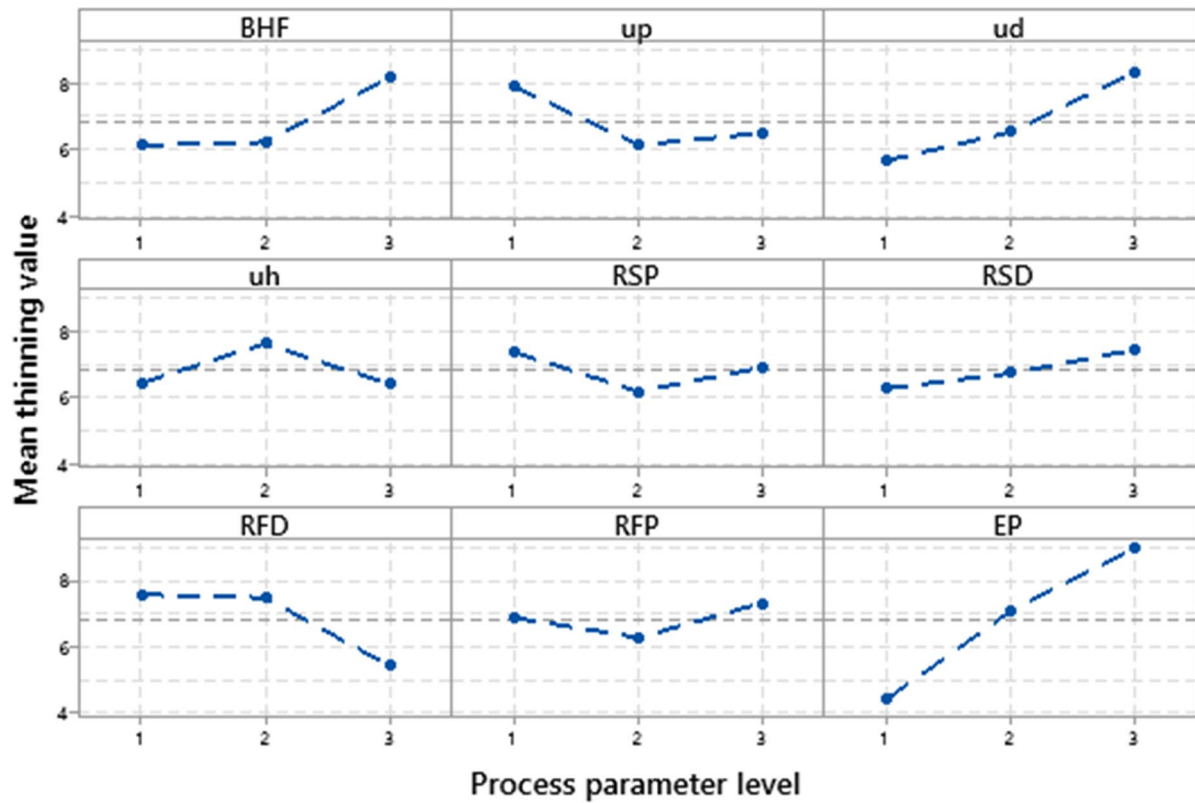


Fig. 12 Main effect of design variables on thinning for DC06 case

cup deep drawing process. The effects of nine important process parameters including blank holder force, punch section radius, die section radius, die fillet radius, punch fillet radius, blank thickness, friction coefficient between punch/blank, die/blank, and blank-holder/blank on the formability of aluminum, advanced high strength steel, and mild steel are studied. In this article, the forming quality characteristic is represented by rupture and thinning, and the readings of rupture and thinning obtained were transformed into a signal-to-noise ratio. The research provided a deeper understanding of the deep drawing of aluminum and high-strength steel sheet metal blanks. As a result, some of the key findings of this survey include:

- The die fillet radius was found to be the main factor affecting rupture for the three selected materials, followed by friction coefficient between blank/die. The results of this study showed that the rupture tends to increase with the increase of the friction coefficient between blank/die, while it increases with the decrease of the die fillet radius.

- The blank thickness was found to be the major factor affecting thinning for the three selected materials, followed by die fillet radius and friction coefficient between blank/die. It is concluded that the thinning tends to increase with an increase in blank thickness and the friction coefficient between blank/die, while the inverse relation exists between the mean value of thinning and die fillet radius.
- It is concluded that the higher the material strength, the lower the thinning value. On the other hand, the higher the strength of the material, the higher the risk of rupture.

A more effective optimization of the deep drawing parameters can be established based on the contribution degree of the factors on the quality of the drawn part. For this reason, the first six parameters, namely, punch section radius, blank holder force, die section radius, die fillet radius, punch fillet radius, and blank thickness need to be carefully monitored or engineered.

## Appendix

**Table 8** L27 designed array for experiments

Exp. no	<i>BHF</i>	$\mu_p$	$\mu_d$	$\mu_h$	$R_{Sp}$	$R_{Sd}$	$R_{Fd}$	$R_{Fp}$	$E_p$
1	10	0.1	0.05	0.05	8	10	4	6	0.8
2	10	0.1	0.05	0.05	12	14	6	10	1.2
3	10	0.1	0.05	0.05	16	18	8	14	1.6
4	10	0.2	0.15	0.15	8	10	4	10	1.2
5	10	0.2	0.15	0.15	12	14	6	14	1.6
6	10	0.2	0.15	0.15	16	18	8	6	0.8
7	10	0.3	0.25	0.25	8	10	4	14	1.6
8	10	0.3	0.25	0.25	12	14	6	6	0.8
9	10	0.3	0.25	0.25	16	18	8	10	1.2
10	30	0.1	0.15	0.25	8	14	8	6	1.2
11	30	0.1	0.15	0.25	12	18	4	10	1.6
12	30	0.1	0.15	0.25	16	10	6	14	0.8
13	30	0.2	0.25	0.05	8	14	8	10	1.6
14	30	0.2	0.25	0.05	12	18	4	14	0.8
15	30	0.2	0.25	0.05	16	10	6	6	1.2
16	30	0.3	0.05	0.15	8	14	8	14	0.8
17	30	0.3	0.05	0.15	12	18	4	6	1.2
18	30	0.3	0.05	0.15	16	10	6	10	1.6
19	60	0.1	0.25	0.15	8	18	6	6	1.6
20	60	0.1	0.25	0.15	12	10	8	10	0.8
21	60	0.1	0.25	0.15	16	14	4	14	1.2
22	60	0.2	0.05	0.25	8	18	6	10	0.8
23	60	0.2	0.05	0.25	12	10	8	14	1.2
24	60	0.2	0.05	0.25	16	14	4	6	1.6
25	60	0.3	0.15	0.05	8	18	6	14	1.2
26	60	0.3	0.15	0.05	12	10	8	6	1.6
27	60	0.3	0.15	0.05	16	14	4	10	0.8



**Table 9** Summary of simulation results for fracture

Exp. no	Simulation results			S/N ratios results		
	DP600	AL-6111-T4	DC06	DP600	AL-6111-T4	DC06
1	1625.18	1086.08	1349.84	-64.22	-60.72	-62.61
2	1542.09	880.64	1295.05	-63.76	-58.90	-62.25
3	1463.23	745.28	1254.13	-63.31	-57.45	-61.97
4	1697.69	1045.02	1429.81	-64.60	-60.38	-63.11
5	1597.56	865.78	1353.52	-64.07	-58.75	-62.63
6	1505.98	873.37	1292.57	-63.56	-58.82	-62.23
7	1848.24	1035.88	1538.34	-65.34	-60.31	-63.74
8	1746.12	1075.96	1499.50	-64.84	-60.64	-63.52
9	1550.94	844.60	1335.24	-63.81	-58.53	-62.51
10	1567.20	984.12	1383.87	-63.90	-59.86	-62.82
11	1889.63	1190.59	1588.19	-65.53	-61.52	-64.02
12	1748.18	1021.40	1639.97	-64.85	-60.18	-64.30
13	1586.81	889.44	1363.28	-64.01	-58.98	-62.69
14	1886.53	1154.07	1667.93	-65.51	-61.24	-64.44
15	1835.71	1187.54	1562.89	-65.28	-61.49	-63.88
16	1388.85	762.96	1253.38	-62.85	-57.65	-61.96
17	1714.35	1152.42	1438.79	-64.68	-61.23	-63.16
18	1614.66	960.36	1374.13	-64.16	-59.65	-62.76
19	2120.01	1399.83	1398.11	-66.53	-62.92	-62.91
20	1740.72	1052.92	1812.78	-64.81	-60.45	-65.17
21	2063.15	1208.73	1946.53	-66.29	-61.65	-65.79
22	1687.69	1181.69	1598.25	-64.55	-61.45	-64.07
23	1465.24	819.61	1337.32	-63.32	-58.27	-62.53
24	1854.21	1290.15	1578.94	-65.36	-62.21	-63.97
25	1435.78	950.14	888.17	-63.14	-59.56	-58.97
26	1552.77	918.13	1344.48	-63.82	-59.26	-62.57
27	1820.79	1259.05	1615.67	-65.21	-62.00	-64.17

**Table 10** Summary of simulation results for thinning

Exp. no	Simulation results			S/N ratios results		
	DP600	AL-6111-T4	DC06	DP600	AL-6111-T4	DC06
1	3.34	2.45	3.98	-10.48	-7.78	-12.00
2	4.45	2.49	5.66	-12.97	-7.93	-15.05
3	5.29	2.71	7.14	-14.47	-8.66	-17.08
4	5.50	3.25	6.41	-14.80	-10.24	-16.13
5	6.32	3.25	7.71	-16.02	-10.25	-17.74
6	2.86	1.64	3.54	-9.11	-4.30	-10.99
7	8.90	4.49	10.22	-18.98	-13.04	-20.19
8	4.01	2.47	4.76	-12.06	-7.85	-13.56
9	4.48	2.30	5.51	-13.02	-7.23	-14.82
10	4.50	3.37	5.24	-13.06	-10.56	-14.38
11	8.12	6.20	9.59	-18.19	-15.85	-19.64
12	3.43	3.00	4.76	-10.71	-9.54	-13.55
13	6.41	3.71	7.52	-16.13	-11.38	-17.53
14	4.14	3.16	5.26	-12.34	-10.00	-14.42
15	6.03	4.46	7.05	-15.61	-12.99	-16.96
16	2.43	1.23	2.97	-7.72	-1.80	-9.46
17	5.14	3.34	6.00	-14.22	-10.48	-15.56
18	6.12	3.35	7.48	-15.73	-10.51	-17.48
19	15.34	9.44	15.56	-23.72	-19.50	-23.84
20	3.19	3.34	5.53	-10.07	-10.49	-14.86
21	7.04	7.22	13.55	-16.95	-17.17	-22.64
22	3.36	2.78	4.39	-10.53	-8.89	-12.85
23	3.59	2.14	4.32	-11.10	-6.63	-12.72
24	7.58	5.41	8.86	-17.60	-14.66	-18.95
25	12.28	2.66	10.06	-21.78	-8.49	-20.05
26	5.84	3.31	6.91	-15.33	-10.39	-16.79
27	3.61	2.80	4.42	-11.16	-8.94	-12.91

**Data availability** The authors declare the availability of data and material.

**Code availability** Not applicable.

## Declarations

**Ethics approval** The article involves no studies on human or animal subjects.

**Consent to participate** Informed consent was obtained from all individual participants included in the study.

**Consent for publication** The publisher has the permission of the authors to publish the given article.

**Competing interests** The authors declare no competing interests.

## References

- Zhang Q, Liu Y, Zhang Z (2016) A new optimization method for sheet metal forming processes based on an iterative learning control model. *Int J Adv Manuf Technol* 85:1063–1075. <https://doi.org/10.1007/s00170-015-7975-4>
- Shafiee Sabet A, Domitner J, Öksüz KI, Hodžić E, Torres H, Rodríguez Ripoll M, Sommitsch C (2021) Tribological investigations on aluminum alloys at different contact conditions for simulation of deep drawing processes. *J Manuf Process* 68:546–557. <https://doi.org/10.1016/j.jmapro.2021.05.050>
- Ma BL, Wan M, Wu XD, Cai ZY, Diao KS, Han JQ (2017) Investigation on forming limit of advanced high strength steels (AHSS) under hot stamping conditions. *J Manuf Process* 30:320–327. <https://doi.org/10.1016/j.jmapro.2017.10.001>
- El Mrabti I, El Hakimi A, Touache A, Chamat A (2022) A comparative study of surrogate models for predicting process failures during the sheet metal forming process of advanced high-strength steel. *Int J Adv Manuf Technol*. <https://doi.org/10.1007/s00170-022-09319-5>

5. Atul ST, Babu MCL (2019) A review on effect of thinning, wrinkling and spring-back on deep drawing process. *Proc Inst Mech Eng Part B J Eng Manuf* 233:1011–1036. <https://doi.org/10.1177/0954405417752509>
6. Raju S, Ganesan G, Karthikeyan R (2013) Sensitivity analysis and statistical process optimisation of deep drawing of AA 6061 sheet material. *Mater Sci Technol* 29:573–580. <https://doi.org/10.1179/1743284712Y.0000000185>
7. Wu L, Zhao C, Cao M, Han X (2021) Effect of ultrasonic and low frequency vibrations on friction coefficient at die radius in deep drawing process. *J Manuf Process* 71:56–69. <https://doi.org/10.1016/j.jmapro.2021.09.008>
8. Dilmeç M, Arap M (2016) Effect of geometrical and process parameters on coefficient of friction in deep drawing process at the flange and the radius regions. *Int J Adv Manuf Technol* 86:747–759. <https://doi.org/10.1007/s00170-015-8225-5>
9. Kardan M, Parvizi A, Askari A (2018) Influence of process parameters on residual stresses in deep-drawing process with FEM and experimental evaluations. *J Braz Soc Mech Sci Eng* 40:157. <https://doi.org/10.1007/s40430-018-1085-9>
10. Jeong HS, Park SH, Cho WS (2019) Influence of process variables on the stamping formability of aluminum wing nose rib. *Int J Precis Eng Manuf* 20:497–510. <https://doi.org/10.1007/s12541-019-00112-1>
11. El Mrabti I, Touache A, El Hakimi A, Chamat A (2021) Spring-back optimization of deep drawing process based on FEM-ANN-PSO strategy. *Struct Multidiscip Optim*. <https://doi.org/10.1007/s00158-021-02861-y>
12. Ayari F, Bayraktar E (2011) Parametric finite element analysis for a square cup deep drawing process. *J Achiev Mater Manuf Eng* 64–86
13. Singh CP, Kanherkar P, Bajpai L, Agnihotri G (2020) Investigation of influence of process parameters in deep drawing of square cup. *AdvEng Optim Intell Tech* 589–598. [https://doi.org/10.1007/978-981-13-8196-6\\_51](https://doi.org/10.1007/978-981-13-8196-6_51)
14. Gutiérrez Regueras JM, Camacho López AM (2014) Investigations on the influence of blank thickness (t) and length/wide punch ratio (LD) in rectangular deep drawing of dual-phase steels. *Comput Mater Sci* 91:134–145. <https://doi.org/10.1016/j.commatsci.2014.04.024>
15. Choudhari CS, Khasbage SS (2021) Experimental investigation of forming parameters for square cup deep drawing process. *Mater Today Proc* 44:4261–4267. <https://doi.org/10.1016/j.matpr.2020.10.543>
16. Mckay MD, Beckman RJ, Conover WJ (2000) A comparison of three methods for selecting values of input variables in the analysis of output from a computer code. *Technometrics* 42:55–61. <https://doi.org/10.1080/00401706.2000.10485979>
17. G. Taguchi, S. Konish (1987) Taguchi method, orthogonal arrays and linear graphs, *Tools for Quality Engineering*. Am Supplier Inst 35–38
18. Danckert J (1995) Experimental investigation of a square-cup deep-drawing process. *J Mater Process Technol* 50:375–384. [https://doi.org/10.1016/0924-0136\(94\)01399-L](https://doi.org/10.1016/0924-0136(94)01399-L)
19. Özek C, Ünal E (2011) Optimization and modeling of angular deep drawing process for square cups. *Mater Manuf Process* 26:1117–1125. <https://doi.org/10.1080/10426914.2010.532526>
20. Xiong P-Y, Almarashi A, Dhahad HA, Alawee WH, Issakhov A, Chu Y-M (2021) Nanoparticles for phase change process of water utilizing FEM. *J Mol Liq* 334:116096. <https://doi.org/10.1016/j.molliq.2021.116096>
21. Shen B, Chen Y, Li C, Wang S, Chen X (2021) Superconducting fault current limiter (SFCL): Experiment and the simulation from finite-element method (FEM) to power/energy system software. *Energy* 234:121251. <https://doi.org/10.1016/j.energy.2021.121251>
22. Chee AKW (2022) The mechanistic determination of doping contrast from Fermi level pinned surfaces in the scanning electron microscope using energy-filtered imaging and calculated potential distributions. *Microsc Microanal* 28:1538–1549. <https://doi.org/10.1017/S1431927622000642>
23. Keeler SP (Stuart P) (1961) Plastic instability and fracture in sheets stretched over rigid punches. Thesis, Mass Inst Technol
24. Zhang R, Shao Z, Lin J (2018) A review on modelling techniques for formability prediction of sheet metal forming. *Int J Lightweight Mater Manuf* 1:115–125. <https://doi.org/10.1016/j.ijlmm.2018.06.003>
25. López AMC, Regueras JMG (2017) Formability of dual-phase steels in deep drawing of rectangular parts: Influence of blank thickness and die radius. *AIP Conf Proc* 1896:020026. <https://doi.org/10.1063/1.5007983>

**Publisher's note** Springer Nature remains neutral with regard to jurisdictional claims in published maps and institutional affiliations.

Springer Nature or its licensor (e.g. a society or other partner) holds exclusive rights to this article under a publishing agreement with the author(s) or other rightsholder(s); author self-archiving of the accepted manuscript version of this article is solely governed by the terms of such publishing agreement and applicable law.